Preprint Cambridge Centre for Computational Chemical Engineering ISSN 1473 – 4273

Numerical simulation of the evolution of soot precursor particles in a laminar ethylene diffusion flame

Edward K. Y. Yapp[1], Jethro Akroyd[1], Sebastian Mosbach[1], Anthony Knobel[1], Alastair J. Smith[1], Dongping Chen[1], Erin M. Webster[2], J. Houston Miller[2], Markus Kraft[1]

released: 10 December 2013

[1] Department of Chemical Engineering
and Biotechnology
University of Cambridge
New Museums Site
Pembroke Street
Cambridge, CB2 3RA
United Kingdom
E-mail: mk306@cam.ac.uk

[2] Department of Chemistry
The George Washington University
Washington, DC 20052
USA
E-mail: houston@gwu.edu

Preprint No. 136

Keywords: Soot, Numerical simulation, Stabilomer, PAH, Diffusion flame

Edited by
Computational Modelling Group
Department of Chemical Engineering and Biotechnology
University of Cambridge
New Museums Site
Pembroke Street
Cambridge CB2 3RA
United Kingdom

Fax: + 44 (0)1223 334796
E-Mail: c4e@cam.ac.uk
World Wide Web: http://como.cheng.cam.ac.uk/

Abstract

A detailed population balance model is used to investigate the physical and chemical evolution of nascent soot particles and their subsequent transformation to carbonaceous aggregates along the centerline of a laminar ethylene co-flow diffusion flame. The model incorporates the aggregate structure of particles and includes detailed compositional knowledge of the individual primary particles that constitute an aggregate. It thereby extends the range of comparisons that can be made with experimental measurements. The carbonisation process is studied using transmission electron microscope-like projections of aggregates and computed C/H ratio and fringe length distributions of the polycyclic aromatic hydrocarbons (PAHs) within the aggregates. Computed C_xH_y (x = 10 to 42 and y = 8 to 16) structures within particles are compared to the most thermodynamically stable aromatics (stabilomers) and a good correspondence is found. The overall model predicts the formation of aggregates between heights of 35 and 45 mm above burner where there is a rapid increase in both the number and diameter of primary particles in each aggregate, and a corresponding increase in the C/H ratio as a result of dehydrogenation reactions. The computed mode of the fringe length distribution shifts towards larger values with particle age. While some of the comparisons between numerical simulations and experimental data is satisfactory, the results of this study shows that further work is required to improve the soot chemistry model, particularly the oxidation rates on different surface site types.

Contents

1 Introduction

The study of soot formation in laminar diffusion flames continues to be a subject of much interest (see, for example, [13, 22]). These flames allow the mechanism of soot formation to be studied in a multidimensional system while avoiding complications in the interpretation of results caused by turbulence. A suite of diagnostic tools have been developed over the last few decades to provide quantitative information on the formation, growth and oxidation of soot. More than 30 years ago, *ex situ* analysis of transmission electron microscopy (TEM) images [6] was first used to find the fractal dimension of aggregates, but the image analysis is based on a 2-D projection. This led to the use of *in situ* light scattering measurements [35] which probe the entire structure of the aggregate; however, the scattering intensity is dependent on the refractive index of soot which is not well-understood. In addition to TEM images which show the morphology of a soot particle, the higher magnification provided by high-resolution transmission electron microscope (HRTEM) [18] has been used for the last 15 years to reveal some details of the internal structure of the particle. A variety of spectroscopic methods exist, for instance, photo-ionisation mass spectroscopy (PIMS) [11] which uses a relatively soft fragmentation technique to monitor the chemical composition of the particle. More recently, efforts have been made to relate Raman [12] and optical band gap [16, 33] measurements to the electronic structure of polycyclic aromatic hydrocarbons (PAHs) within the particles.

Much progress has been made in developing the modelling capabilities to accurately predict soot formation in laminar diffusion flames. The majority of works are based on spherical [27] or surface-volume [22] soot models solved using a sectional method. These types of particle models are appropriate under certain conditions. But it has been demonstrated, albeit for silica and silicon nanoparticle systems, that substantial errors can be incurred when a particle model inappropriate for a particular modelling application is used [15]. Detailed population balance models solved using a stochastic method have been utilised. The model used in this work [3, 4, 20, 21, 24] incorporates the aggregate structure of soot particles by resolving the geometry and composition of individual primary particles and their connectivity to other primary particles in an aggregate. This allowed us to create TEM-like projections of aggregates and to determine the evolution of the fractal dimension in flames [17]. Each primary particle contains individual PAH species. By describing the structure and growth of these PAHs comparisons have been made between computed and experimental PAH mass spectra to study the collision efficiency of PAHs [21].

The **purpose of this paper** is to use a detailed population balance model to resolve the distribution of PAHs in particles, simulate TEM images of aggregates, and compute fringe length distributions, C/H ratio distributions and the conjugation length of PAHs in particles for the laminar ethylene co-flow diffusion flame. The main objective is to investigate the carbonisation process along the centerline of the flame and to identify areas of further work.

2 Computational method

In the work performed by Smooke and co-workers [12], temperature and species fields were computed for four flames of different ethylene and nitrogen fuel mixtures. In their model the species, energy and fluid dynamic equations were coupled with a spherical soot particle model solved using a sectional method. The spherical sectional soot model [27] approximately accounts for the production and consumption of key gas-phase species due to surface growth and oxidation. In the present paper, temperature and species profiles were extracted along the streamlines of the simulated flames and were supplied as input to the detailed population model [4].

3 Detailed population balance model

Figure 1 gives an overview of the major processes considered in the detailed population balance model. The gas-phase chemistry is computed up to A1 (benzene) using a modified version of GRI-Mech 1.2 [29] and a steady-state expression is used for the formation rate of A2 (naphthalene) which depends on the C_2H_2, H_2 and C_6H_5 concentrations [26]. The detailed model, or specifically, the kinetic Monte-Carlo-aromatic site (KMC-ARS) model [20], describes the growth of PAH species beyond A2. The dynamics of the soot particle population is described by the Smoluchowski equation [9, 10, 25] with additional terms for particle inception, surface growth, condensation and sintering. The evolution of PAHs in the gas phase is coupled to the evolution of PAHs within an aggregate as shown in the figure. A detailed description of the particle model [4, 20, 24] and the numerical method used to simulate the population dynamics [2, 19] may be found in the existing literature. A brief description of the most important aspects of the model is given below.

Soot particles are represented as aggregates composed of primary particles, where each primary is composed of a number of PAHs [24]. A PAH is represented by the number of carbon and hydrogen atoms it contains, and the number and type of each elementary site defined by the shape of its edge [20]. These elementary sites include free-edge, zig-zag, armchair and bay sites [3, 8]. This representation allows the structure, fringe length (defined as the largest carbon-carbon pair distance) and conjugation length (a function of the number of aromatic rings) of each individual PAH to be resolved. A primary particle is represented as a set of two or more PAHs. An aggregate is represented as a set of two or more primary particles. Each aggregate stores a list of neighbouring primary particles and resolves the shared surface area between each pair of neighbours. This description allows the model to resolve whether each pair of neighbours is in point contact, fully coalesced or somewhere in between [24]. The level of coalescence is described by a *sintering level* [23]. A sintering level of 0 corresponds to point contact and a sintering level of 1 corresponds to complete coalescence.

There are five different particle processes in the model:

Inception A primary particle is formed when two PAHs stick following a collision. The sticking probability of these two PAHs is determined by a simple collision efficiency model [4]. If the sum of the masses of the collision partners exceeds a given

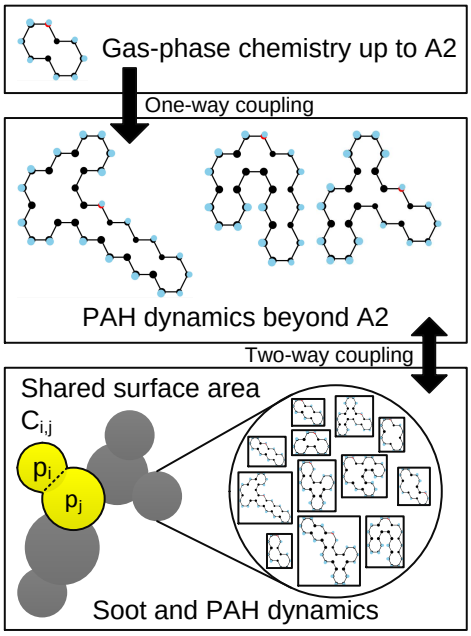

Figure 1: *Coupling between the gas and particle phases in the detailed population balance model.*

threshold, then they will stick. This implies a unity sticking probability for particles that exceed this mass.

Coagulation An aggregate is formed when two (primary or aggregate) particles stick following a collision. The rate of collision is determined by a transition regime coagulation kernel [19] which is dependent on the mass and collision diameter of each collision partner. After a coagulation event, two primary particles (one from each collision partner) are assumed to be in point contact. These primaries may undergo subsequent particle rounding due to mass addition [24] via surface growth and condensation, and due to sintering [23].

Surface growth PAHs in a (primary or aggregate) particle may grow via surface reactions with gas-phase species. The rate of surface growth is a function of the structure of the PAH and is described by the KMC-ARS model. Two parameters are introduced to differentiate the rate of growth of PAHs in a particle versus those in the gas phase. The *growth factor* $g \in [0,1]$ [24] is a multiplier that is applied to the growth rate of PAHs within particles when the number of PAHs exceeds a critical value, n_{crit}. It is intended to account for the possibility that PAHs in large particles grow more slowly than PAHs in the gas phase.

Surface growth increases the mass of a PAH, which results in an increase in the sphericity of the primary particle containing the PAH and any neighbouring primary particles [24]. This particle rounding takes the form of an increase in the shared surface area between the affected primary particles. The rate of particle rounding is parameterised by a *smoothing factor* $s \in [0,2]$ [24] that relates the change of the shared surface area to the change of the volume of a primary particle. A smoothing factor of 0 implies instantaneous coalescence, whereas a smoothing factor of 2

implies no rounding.

Condensation Primary particles or aggregates may grow via condensation of a gas-phase PAH, following a collision between the PAH and a primary or aggregate particle. The rate of collision is calculated as per coagulation, except that one of the collision partners is a molecule. Rounding by mass addition occurs via the same mechanism as described for the surface growth process above.

Sintering Neighbouring primary particles may undergo particle rounding via a sintering process. The rate of sintering between each pair of neighbouring primary particles p_i and p_j is given [23]:

$$\frac{\mathrm{d}C_{i,j}}{\mathrm{d}t} = -\frac{1}{\tau_\mathrm{s}}(C_{i,j} - S_{i,j}), \tag{1}$$

where $C_{i,j}$ is the shared surface area (highlighted in Fig. 1) of primary particles p_i and p_j, and $S_{i,j}$ is the surface area of a sphere with the same volume as primaries p_i and p_j. The characteristic sintering time is given [31]:

$$\tau_\mathrm{s} = A d_{i,j} \exp\left[\frac{E}{T}\left(1 - \frac{d_\mathrm{crit}}{d_{i,j}}\right)\right], \tag{2}$$

where A is the pre-exponential factor, $d_{i,j}$ is the minimum diameter of two neighbouring primary particles, E is the activation energy and d_crit is the critical diameter for sintering. For $d_{i,j} < d_\mathrm{crit}$, sintering is assumed to be instantaneous.

Three key changes were made to the soot chemistry model to match the experimental soot volume fraction:

1. A zig-zag oxidation reaction by OH (rate based on benzene oxidation [32]) was added. An ad-hoc assumption of this type is required for the complete oxidation of soot particles in the post-flame region.

2. A factor of 4 was applied to the surface growth rate (as inspired by Smooke et al. [27]).

3. A g of 0.75 was used.

A threshold of 48 carbon atoms in the collision efficiency model (dimerisation of species equal in size to coronene or larger) and the set of optimised model parameters found by Chen et al. [4] was used. To track the exact structure of each PAH in the gas-phase and within particles requires considerable CPU time and memory. A stochastic weight of 32 (unless otherwise indicated) was attached to each computational PAH in order to reduce the memory requirement of the computer code to an acceptable level. This means that each computational PAH represents 32 real PAHs. The model output was found to be insensitive over a wide range of stochastic weights.

4 Results and discussion

4.1 Soot volume fraction

The soot volume fraction was measured experimentally using two-dimensional laser-induced incandescence (LII) by Herdman et al. [12] for four different ethylene and nitrogen fuel mixtures.

Figure 2 shows a comparison of the experimental and computed soot volume fraction profile along the centerline of the flame with a fuel mixture of 60 % ethylene and 40 % nitrogen (by volume). The model is in good agreement with the experimental peak soot volume fraction; however, the predicted distribution is narrower and located further along the centerline. A potential explanation for this discrepancy is the implicit assumption made in the postprocessing method that there is no diffusive or thermophoretic transport of gas-phase species or particles between adjacent streamlines.

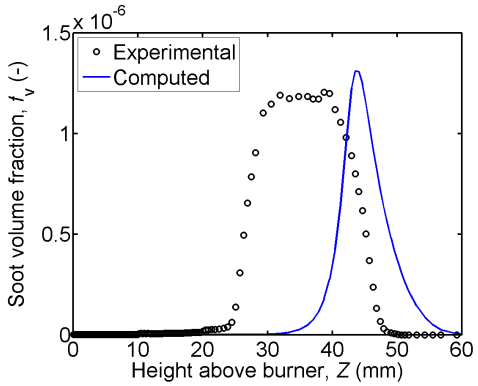

Figure 2: *Comparison between the experimental (symbols) and computed (line) soot volume fraction along the centerline of the ethylene diffusion flame.*

4.2 Stabilomer grid of Stein and Fahr

The detailed population balance model resolves the mass of each PAH. As shown in **Fig.** 3, this allows us to provide computed mass spectra to enable direct comparison with experimental observations made using PIMS [11]. The computed PAH masses can be presented on the stabilomer grid which represents the most stable C_xH_y species ($10 \leq x \leq 42$ and $8 \leq y \leq 16$ for even values of x and y) identified by Stein and Fahr [28].

Table 1 presents the count fractions of computed PAHs in the particle phase on the stabilomer grid (shown as the shaded area) for heights above burner (HAB) of Z = 25 and 35 mm. Most of the count fractions appear in the shaded area which shows that many of the computed PAH structures are identical in mass to stabilomers. The bottom-right corner of the shaded area is populated with an increase in HAB which implies that the growth of PAHs to larger sizes takes place along the stabilomer grid. It may be noted that about 10–30 % of the computed PAH structures does fall below the stabilomer grid. These

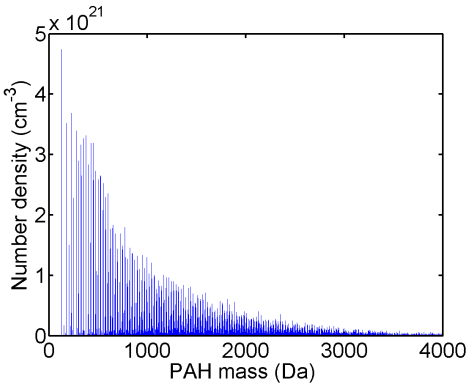

Figure 3: *Computed PAH mass spectrum at height above burner Z = 35 mm.*

structures correspond to PAHs which undergo only free-edge ring growth [20]. According to the kinetic analysis performed by Frenklach [7], high temperatures are conducive to the formation of stabilomers [7]. Because the temperature (and H_2 concentration) for $Z \leq 35$ mm is low, PAH growth is controlled by the rate of H abstraction [7].

Carbon number, x

Hydrogen number, y	10	12	14	16	18	20	22	24	26	28	30	32	34	36	38	40	42	Σ
8	10	0.4	≈0															10
10			7.4	3.2	0.8	0.2												12
12					7.8	4.8	4.6	1.5	0.5	0.2								19
14							7.2	6.1	6.7	4.5	2.2	0.8	0.3	0.1				28
16									5.6	6.9	7.0	4.8	3.2	2.0	0.8	0.5	0.3	31
Σ	10	0.4	7.5	3.2	8.6	5.0	12	7.6	13	12	9.2	5.6	3.6	2.0	0.8	0.5	0.3	100

z = 35 mm

Carbon number, x

Hydrogen number, y	10	12	14	16	18	20	22	24	26	28	30	32	34	36	38	40	42	Σ
8	32	0.4																32
10			27	7.2	0.4													34
12					15	2.5	1.1	0.4										19
14							8.2	1.8		0.4								10
16									4.7						0.4			5.0
Σ	32	0.4	27	7.2	15	2.5	9.3	2.2	4.7	0.4					0.4			100

z = 25 mm

Table 1: *Percentage distribution of computed PAHs in the particle phase presented on the stabilomer grid (shaded area) at various heights in the ethylene diffusion flame. The numbers represent the count of each computed C_xH_y normalised by the total count over all values of x and y.*

4.3 Carbonisation process

Figure 4 shows various aspects of the soot morphology calculated from the detailed population balance model: (a) TEM images which track the evolution of a representative particle along the flame, (b) fringe length distributions of the corresponding particle and (c) C/H ratio of PAHs in the particle phase for Z = 35, 40 and 45 mm.

The TEM images (left panel) show that the transition from a single spherical primary particle to an aggregate takes place between Z = 35 and 40 mm. Once an aggregate is

formed there is a rapid increase in both the number and diameter of primary particles in the aggregate. This is consistent with the rapid carbonisation process that has been observed experimentally [5, 13]. The C/H ratio (right panel) of nascent soot particles is relatively low (the mean C/H ratio indicated by circles lies well below the peri-condensed line). These particles undergo dehydrogenation by unimolecular reaction or abstraction by H or OH which shifts the mean C/H ratio towards the peri-condensed line as the particles age.

The mode of the fringe length distributions (middle panel) shifts towards larger values with particle age. In contrast, young and mature soot sampled from flames of different fuel types display a mode which remains fixed [1]. This discrepancy may be related to the high growth factor (g = 0.75) that was assumed where PAHs within the aggregates continue to grow at a significant rate.

Figure 5 shows a least squares fit of the number of primary particles in an aggregate, N, against the average aggregate size, R, at Z = 45 mm. The aggregate size was defined as the geometric mean of the length, L, and the width, W, normal to L of a 2-D projection of the simulated aggregate. An alternative definition is based on the radius of gyration but is difficult to measure experimentally. Using a simple power law relationship ($N \propto R^{D_f}$), the fractal dimension, D_f, was determined to be 1.68 ± 0.01 which implies elongated, open structures as illustrated by the TEM image in the top-left panel of Fig. 4.

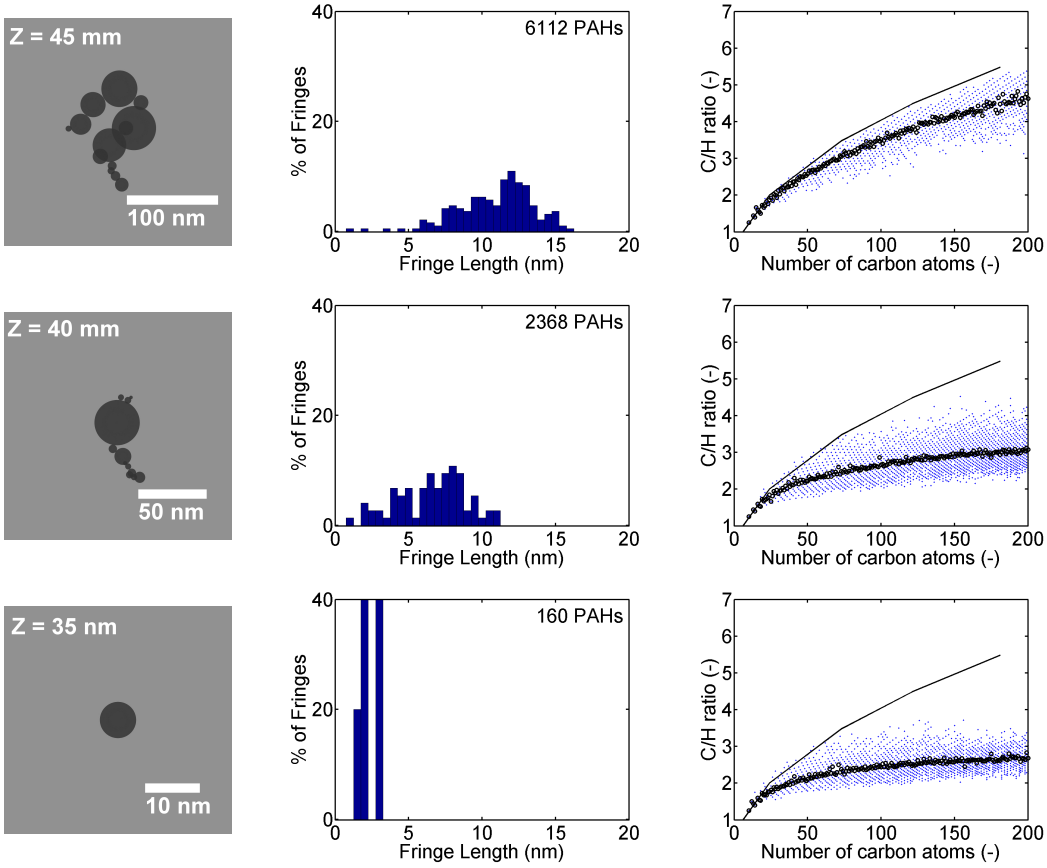

Figure 4: *Left panel: Simulated TEM images tracking the evolution of a representative particle at various heights in the ethylene diffusion flame. Middle panel: Computed fringe length distributions corresponding to the particle in the left panel (the number of PAHs is shown). Right panel: Computed C/H ratio of PAHs in the particle phase (dots). Circles used for the mean ratio for a given number of carbon atoms. Peri-condensed line is shown [34].*

4.4 Conjugation length

In the Raman study by Herdman et al. [12] samples were collected by rapidly inserting a horizontal wire into the flame with a fuel mixture of 60 % ethylene and 40 % nitrogen (by volume) at multiple HAB beginning at 4 mm, in steps of 2 mm, up to 56 mm. At each HAB Raman spectra were obtained across the wire at lateral positions of -40 mm to +40 mm at 1 mm spacing. Raman signals were observed at heights below those where LII was observed, thus leading Herdman et al. [12] to postulate that these signals may be attributable to the smaller particles. The ratio of the D to G band intensities in the Raman spectrum may be related to the conjugation length, L_A, using the phenomenological relationship proposed by Lucchese et al. [14].

In work that has yet to be published [33], light from a supercontinuum white light laser source was focused into the flame with the same fuel mixture as in the Raman study at

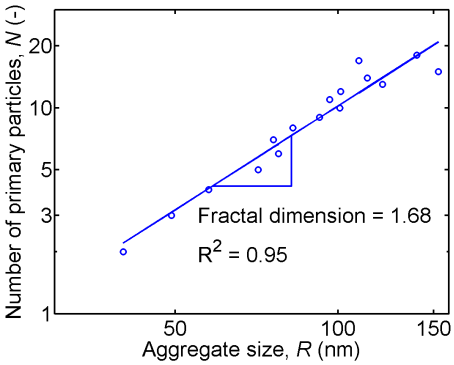

Figure 5: *Number of primary particles in an aggregate versus the average aggregate size for simulated data at Z = 45 mm. $R = (LW)^{1/2}$ where L is the length and W is the width normal to L of a 2-D projection of the simulated aggregate.*

multiple HAB beginning at 10 mm, in steps of 5 mm, up to 40 mm. The transmitted light was directed into a spectrometer and the optical band gap was evaluated from the absorption spectrum by Tauc analysis [30]. The optical band gap may be related to the number of aromatic rings, M, in a molecule using the correlation proposed by Miller et al. [16]. We assumed that the conjugation length is related to the diameter of a circle of equivalent area as the rings:

$$L_{\mathrm{A}} = \left(4 \frac{3^{3/2} a^2}{2\pi} M \right)^{1/2}, \tag{3}$$

where a is the length of an aromatic C–C bond (1.395 Å).

Figure 6 shows a comparison of the experimental and computed conjugation length along the centerline of the flame for $0 \leq Z \leq 30$ mm. Each experimental data point corresponds to an average across a range of radial positions where a Raman spectrum is observed or where a relatively high extinction signal to noise ratio can be obtained at that HAB. Each point along the computed line corresponds to a number average of the largest conjugation length in the small particles (particle masses $\leq$ 1000 Da). The experimental conjugation lengths do not show any systematic variation and correspond to a PAH of approximately 8 aromatic rings (approximately the size of coronene). For $0 \leq Z \leq 21$ mm, all computed PAHs exist in the gas-phase. These PAHs grow and inception occurs at Z = 21 mm. The size of the largest PAH in the small particles does not seem to vary throughout the particle inception zone which is consistent with the experimental observation. The source of the Raman scattering may indeed be attributable to the small particles dominated by relatively small PAHs and the results lend some support to an inception process involving species which are equal in size to coronene or larger.

5 Conclusions

In this paper we have presented a modelling study of the carbonisation process on the centerline of a laminar ethylene co-flow diffusion flame. A detailed population balance

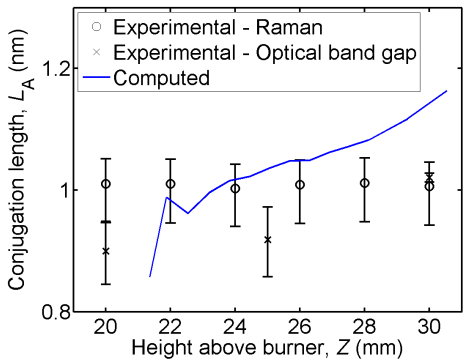

Figure 6: *Comparison between the experimental conjugation length estimated from Raman (circles) and optical band gap (crosses) measurements, which was averaged across a range of radial positions at each HAB, and the computed conjugation length (line) of the small particles along the centerline of the ethylene diffusion flame. A stochastic weight of 1 was used.*

model was used to resolve a range of quantities which may be compared with experimental measurements. In order to predict the experiment soot volume fraction, the following changes were made to the soot chemistry model: (a) introduction of a zig-zag oxidation reaction by OH, (b) enhancement of the surface growth rate of PAHs in the gas-phase and PAHs within primary particles by a factor of 4 and (c) application of a factor of 0.75 to the growth rate of PAHs within primary particles. Under these assumptions the overall model reproduced the experimental peak soot volume fraction but had some difficulty in accurately reproducing the distribution of soot formed. For the first time the thermodynamic stability of computed PAHs in soot particles was investigated through comparisons with Stein's stabilomers. The computed PAH structures are in good agreement with the thermodynamic predictions of the stabilomer grid; furthermore, it was shown that PAHs grow along the stabilomer grid as the particles age.

The overall model was found to qualitatively capture the carbonisation process. The computed particles are initially spherical evolving to aggregates with a fractal dimension of 1.68. The aggregates exhibit a high C/H ratio indicative of a carbonised particle resulting from dehydrogenation reactions. The mode of the computed fringe length distribution shifts towards larger values with particle age as PAHs within the particle were allowed to grow. An appropriate length scale was extracted from the model and compared with the conjugation length derived from Raman and optical band gap measurements. The results suggest that the source of the Raman scattering is attributable to nascent soot particles with relatively small PAH conjugation lengths ($\approx$ 1 nm). Future work is required to better understand the oxidation of soot on different site types and to compare the model against observations of a set of well-characterised flames.

6 Acknowledgements

This publication is made possible by the Singapore National Research Foundation under its Campus for Research Excellence And Technological Enterprise (CREATE) programme. The authors would like to thank Dr. W. J. Menz for advice on improving the performance of the code, Dr. B. C. Connelly, Prof. M. B. Long and Prof. M. D. Smooke for providing the numerical simulations and Ms. J. D. Herdman for the experimental measurements. Financial support by the Gates Cambridge Trust is gratefully acknowledged.

References

[1] M. Alfè, B. Apicella, R. Barbella, J.-N. Rouzaud, A. Tregrossi, and A. Ciajolo. Structure–property relationship in nanostructures of young and mature soot in premixed flames. *Proceedings of the Combustion Institute*, 32:697–704, 2009. doi:10.1016/j.proci.2008.06.193.

[2] M. Celnik, R. Patterson, M. Kraft, and W. Wagner. Coupling a stochastic soot population balance to gas-phase chemistry using operator splitting. *Combustion and Flame*, 148:158–176, 2007. doi:10.1016/j.combustflame.2006.10.007.

[3] M. Celnik, A. Raj, R. West, R. Patterson, and M. Kraft. Aromatic site description of soot particles. *Combustion and Flame*, 155:161–180, 2008. doi:10.1016/j.combustflame.2008.04.011.

[4] D. Chen, Z. Zainuddin, E. Yapp, J. Akroyd, S. Mosbach, and M. Kraft. A fully coupled simulation of PAH and soot growth with a population balance model. *Proceedings of the Combustion Institute*, 34:1827–1835, 2013. doi:10.1016/j.proci.2012.06.089.

[5] R. Dobbins, R. Fletcher, and H.-C. Chang. The evolution of soot precursor particles in a diffusion flame. *Combustion and Flame*, 115:285–298, 1998. doi:10.1016/S0010-2180(98)00010-8.

[6] S. R. Forrest and T. A. Witten. Long-range correlations in smoke-particle aggregates. *Journal of Physics A: Mathematical and General*, 12:L109–L117, 1979. doi:10.1088/0305-4470/12/5/008.

[7] M. Frenklach. On the driving force of PAH production. *Symposium (International) on Combustion*, 22:1075–1082, 1989. doi:10.1016/S0082-0784(89)80117-1.

[8] M. Frenklach. On surface growth mechanism of soot particles. *Symposium (International) on Combustion*, 26:2285–2293, 1996. doi:10.1016/S0082-0784(96)80056-7.

[9] S. Friedlander. *Smoke, dust, and haze*. New York: Oxford University Press, 2000.

[10] N. Fuchs. *The mechanics of aerosols*. New York: Dover, 1989.

[11] J. Happold. *Geschichtete polyzyklische aromatische Kohlenwasserstoffe als Bausteine der Rußbildung*. PhD thesis, Universität Stuttgart, 2008.

[12] J. D. Herdman, B. C. Connelly, M. D. Smooke, M. B. Long, and J. H. Miller. A comparison of Raman signatures and laser-induced incandescence with direct numerical simulation of soot growth in non-premixed ethylene/air flames. *Carbon*, 49: 5298–5311, 2011. doi:10.1016/j.carbon.2011.07.050.

[13] M. Kholghy, M. Saffaripour, C. Yip, and M. J. Thomson. The evolution of soot morphology in a laminar coflow diffusion flame of a surrogate for Jet A-1. *Combustion and Flame*, 160:2119–2130, 2013. doi:10.1016/j.combustflame.2013.04.008.

[14] M. Lucchese, F. Stavale, E. M. Ferreira, C. Vilani, M. Moutinho, R. B. Capaz, C. Achete, and A. Jorio. Quantifying ion-induced defects and Raman relaxation length in graphene. *Carbon*, 48:1592–1597, 2010. doi:10.1016/j.carbon.2009.12.057.

[15] W. J. Menz and M. Kraft. The suitability of particle models in capturing aggregate structure and polydispersity. *Aerosol Science and Technology*, 47:734–745, 2013. doi:10.1080/02786826.2013.788244.

[16] J. H. Miller, J. D. Herdman, C. D. Green, and E. M. Webster. Experimental and computational determinations of optical band gaps for PAH and soot in a N2-diluted, ethylene/air non-premixed flame. *Proceedings of the Combustion Institute*, 34:3669–3675, 2013. doi:10.1016/j.proci.2012.05.054.

[17] N. Morgan, M. Kraft, M. Balthasar, D. Wong, M. Frenklach, and P. Mitchell. Numerical simulations of soot aggregation in premixed laminar flames. *Proceedings of the Combustion Institute*, 31:693–700, 2007. doi:10.1016/j.proci.2006.08.021.

[18] A. B. Palotás, L. C. Rainey, C. J. Feldermann, A. F. Sarofim, and J. B. Vander Sande. Soot morphology: an application of image analysis in high-resolution transmission electron microscopy. *Microscopy research and technique*, 33:266–78, 1996. doi:10.1002/(SICI)1097-0029(19960215)33:3<266::AID-JEMT4>3.0.CO;2-O.

[19] R. I. Patterson, J. Singh, M. Balthasar, M. Kraft, and W. Wagner. Extending stochastic soot simulation to higher pressures. *Combustion and Flame*, 145:638–642, 2006. doi:10.1016/j.combustflame.2006.02.005.

[20] A. Raj, M. Celnik, R. Shirley, M. Sander, R. Patterson, R. West, and M. Kraft. A statistical approach to develop a detailed soot growth model using PAH characteristics. *Combustion and Flame*, 156:896–913, 2009. doi:10.1016/j.combustflame.2009.01.005.

[21] A. Raj, M. Sander, V. Janardhanan, and M. Kraft. A study on the coagulation of polycyclic aromatic hydrocarbon clusters to determine their collision efficiency. *Combustion and Flame*, 157:523–534, 2010. doi:10.1016/j.combustflame.2009.10.003.

[22] M. Saffaripour, A. Veshkini, M. Kholghy, and M. J. Thomson. Experimental investigation and detailed modeling of soot aggregate formation and size distribution in laminar coflow diffusion flames of Jet A-1, a synthetic kerosene, and n-decane. *Combustion and Flame*, pages 1–16, 2013. doi:10.1016/j.combustflame.2013.10.016.

[23] M. Sander, R. H. West, M. S. Celnik, and M. Kraft. A detailed model for the sintering of polydispersed nanoparticle agglomerates. *Aerosol Science and Technology*, 43: 978–989, 2009. doi:10.1080/02786820903092416.

[24] M. Sander, R. I. Patterson, A. Braumann, A. Raj, and M. Kraft. Developing the PAH-PP soot particle model using process informatics and uncertainty propagation. *Proceedings of the Combustion Institute*, 33:675–683, 2011. doi:10.1016/j.proci.2010.06.156.

[25] J. Seinfeld and S. Pandis. *Atmospheric chemistry and physics. From air pollution to climate change*. New York: Wiley, 1998.

[26] M. Smooke, C. Mcenally, L. Pfefferle, R. Hall, and M. Colket. Computational and experimental study of soot formation in a coflow, laminar diffusion flame. *Combustion and Flame*, 117:117–139, 1999. doi:10.1016/S0010-2180(98)00096-0.

[27] M. Smooke, M. Long, B. Connelly, M. Colket, and R. Hall. Soot formation in laminar diffusion flames. *Combustion and Flame*, 143:613–628, 2005. doi:10.1016/j.combustflame.2005.08.028.

[28] S. E. Stein and A. Fahr. High-temperature stabilities of hydrocarbons. *The Journal of Physical Chemistry*, 89:3714–3725, 1985. doi:10.1021/j100263a027.

[29] C. Sun, C. Sung, H. Wang, and C. Law. On the structure of nonsooting counterflow ethylene and acetylene diffusion flames. *Combustion and Flame*, 107:321–335, 1996. doi:10.1016/S0010-2180(96)00055-7.

[30] J. Tauc, R. Grigorovici, and A. Vancu. Optical Properties and Electronic Structure of Amorphous Germanium. *physica status solidi (b)*, 15:627–637, 1966. doi:10.1002/pssb.19660150224.

[31] S. Tsantilis, H. Briesen, and S. E. Pratsinis. Sintering time for silica particle growth. *Aerosol Science and Technology*, 34:237–246, 2001. doi:10.1080/02786820119149.

[32] H. Wang and M. Frenklach. A detailed kinetic modeling study of aromatics formation in laminar premixed acetylene and ethylene flames. *Combustion and Flame*, 110:173–221, 1997. doi:10.1016/S0010-2180(97)00068-0.

[33] E. M. Webster and J. H. Miller. *unpublished results*, 2013.

[34] P. Weilmünster, A. Keller, and K.-H. Homann. Large molecules, radicals, ions, and small soot particles in fuel-rich hydrocarbon flames. *Combustion and Flame*, 116: 62–83, 1999. doi:10.1016/S0010-2180(98)00049-2.

[35] H. X. Zhang, C. M. Sorensen, E. R. Ramer, B. J. Olivier, and J. F. Merklin. In situ optical structure factor measurements of an aggregating soot aerosol. *Langmuir*, 4: 867–871, 1988. doi:10.1021/la00082a015.